

Supplementary Materials for
Kinetic implications of IP₆ anion binding on the molecular switch of HIV-1 capsid assembly

Manish Gupta *et al.*

Corresponding author: Gregory A. Voth, gavoth@uchicago.edu

Sci. Adv. **11**, eadt7818 (2025)
DOI: 10.1126/sciadv.adt7818

The PDF file includes:

Figs. S1 to S10
Legends for movies S1 and S2

Other Supplementary Material for this manuscript includes the following:

Movies S1 and S2

Here, we present results from additional unbiased all-atom simulations of the capsid patch under -IP₆ and +IP₆ conditions. Three replicas were simulated for each case. Without IP₆, the TVGG motif primarily stayed in coil configuration, only transiently exploring the folded conformations. Notably, the central pore is more dynamic in the absence of IP₆, resulting in the relocation of M39 residues towards the 'pawl' state near the TVGG motif, as is evident from the K25-M39 and T58-M39 distance analyses. In the presence of IP₆, M39 preferred to stay in the 'ratchet' state packing against V24/K25, which led to occasional folding of the TVGG motif into a partial 3₁₀-helix conformation.

Replica 2

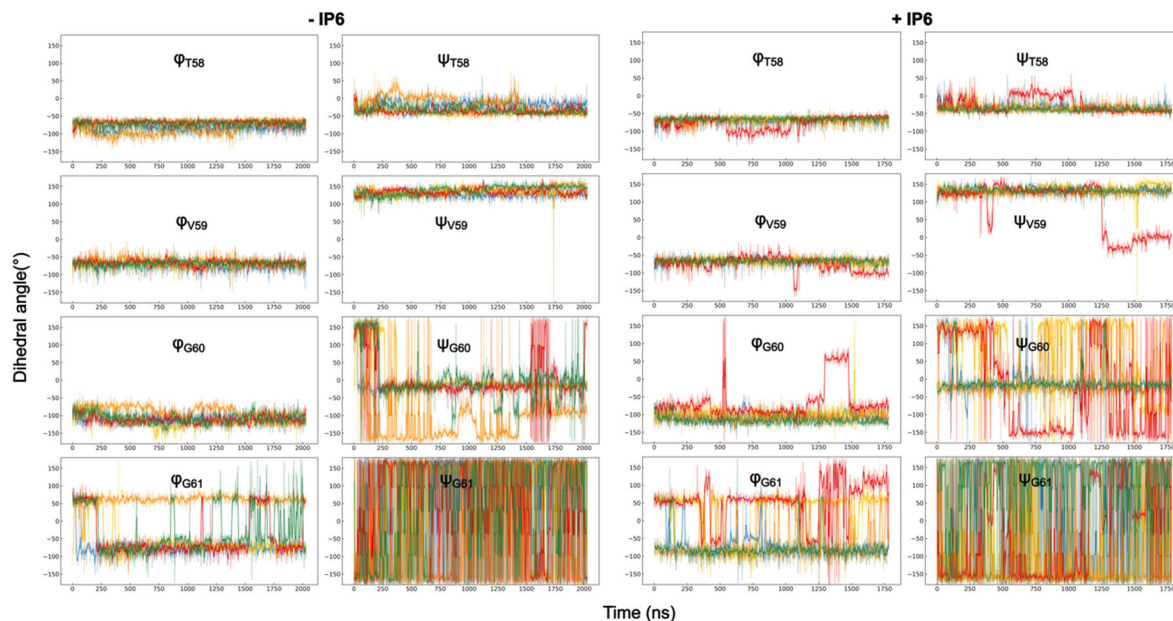


Fig. S1. Time series of the TVGG backbone dihedral angles in the absence (-IP₆) and presence (+IP₆) of IP₆. (-IP₆) T58 residues in the capsid pentamer adopted a folded configuration except for the T58 residue in the γ -domain, which eventually converged to a 3₁₀-helix conformation. V59, G60 residues were ordered but deviated from a typical folded conformation. G61 residues were relatively more mobile. (+IP₆) T58 residue in the α -domain CA unfolded briefly, following which T58 and V59 residues switched to a folded conformation, forming a partial 3₁₀-helix structure.

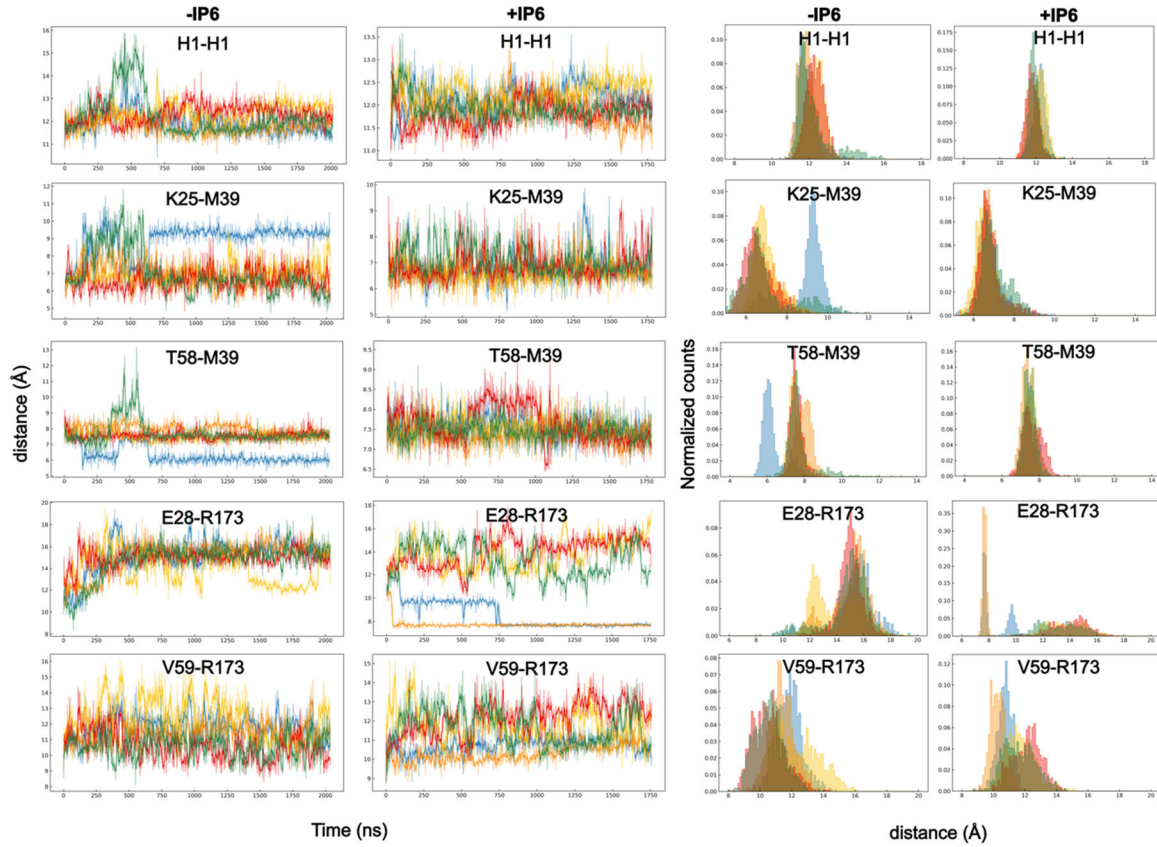


Fig. S2. Time series of the capsid structural network that links IP₆ to the TVGG motif in the absence (-IP₆) and presence (+IP₆) of IP₆. (-IP₆) In this case, the central pore was relatively ordered. In the pentamer, a stable K25/M39 packing was observed between NTD of adjacent CA monomers. However, M39 residue in the β -domain moved away from α -domain V24/K25, breaking the 'ratchet' state preferred in pentamers. (+IP₆) IP₆ stabilized the electrostatic repulsion within the pentamer central pore. This led to an ordered K25 ring accommodating stable packing with M39 of adjacent CA domains. The pentamer did not deviate from 'pawl' conformation during the simulation.

Replica 3

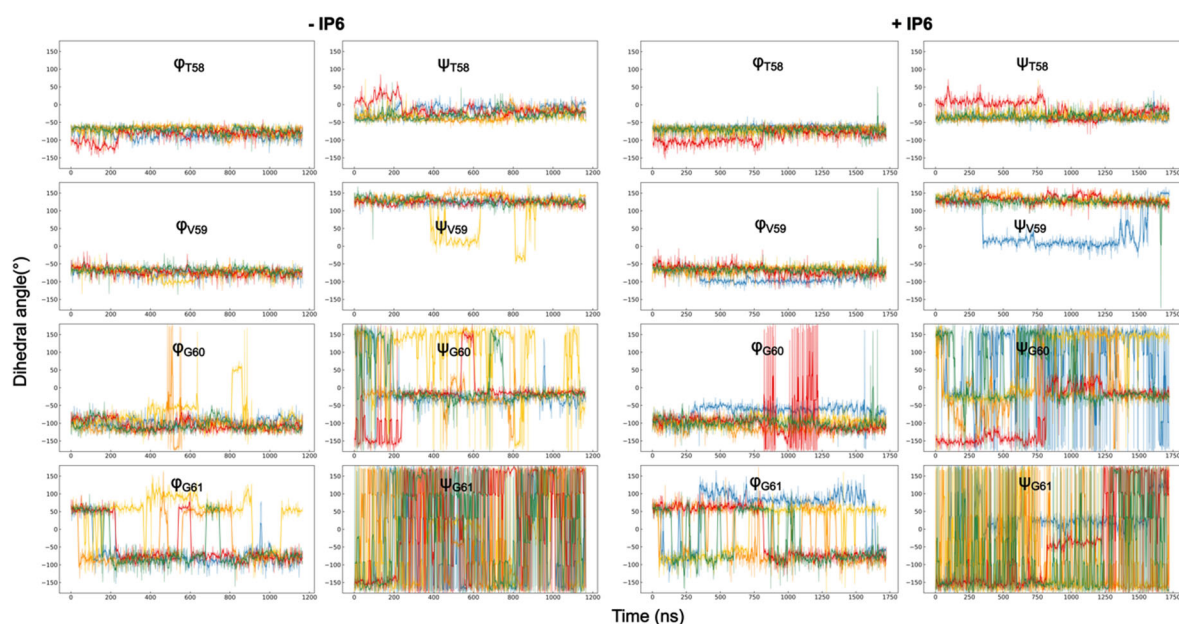


Fig. S3. Time series of the TVGG backbone dihedral angles in the absence (-IP6) and presence (+IP6) of IP6. (+IP6) β -domain V59 residue explored folded conformations transiently, however, all chains converged to coil conformation.

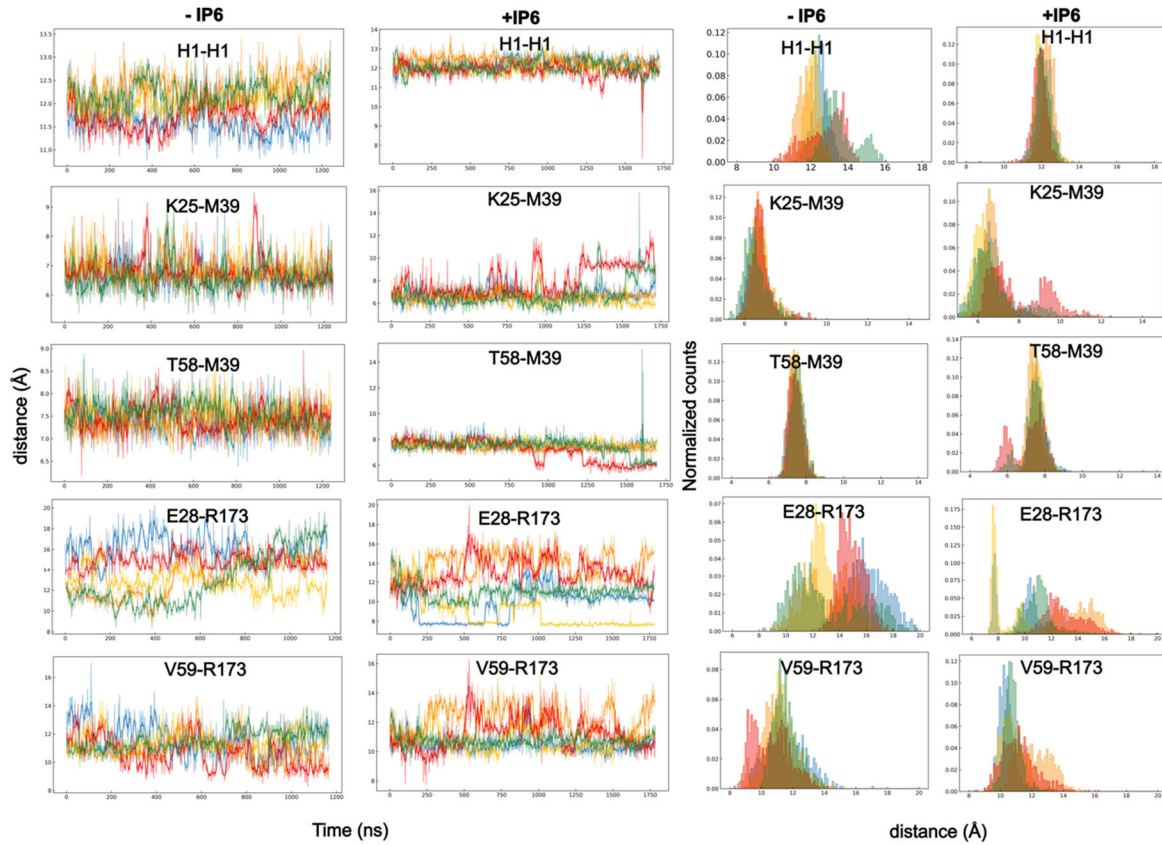


Fig. S4. Time series of the capsid structural network that links IP₆ to the TVGG motif in the absence (-IP₆) and presence (+IP₆) of IP₆. (+IP₆) The capsid pentamer stayed in the 'ratchet' conformation during the time of the simulation which allowed the TVGG motif in the β -domain (Fig. S3) to explore helix-like folded conformations.

Replica 4

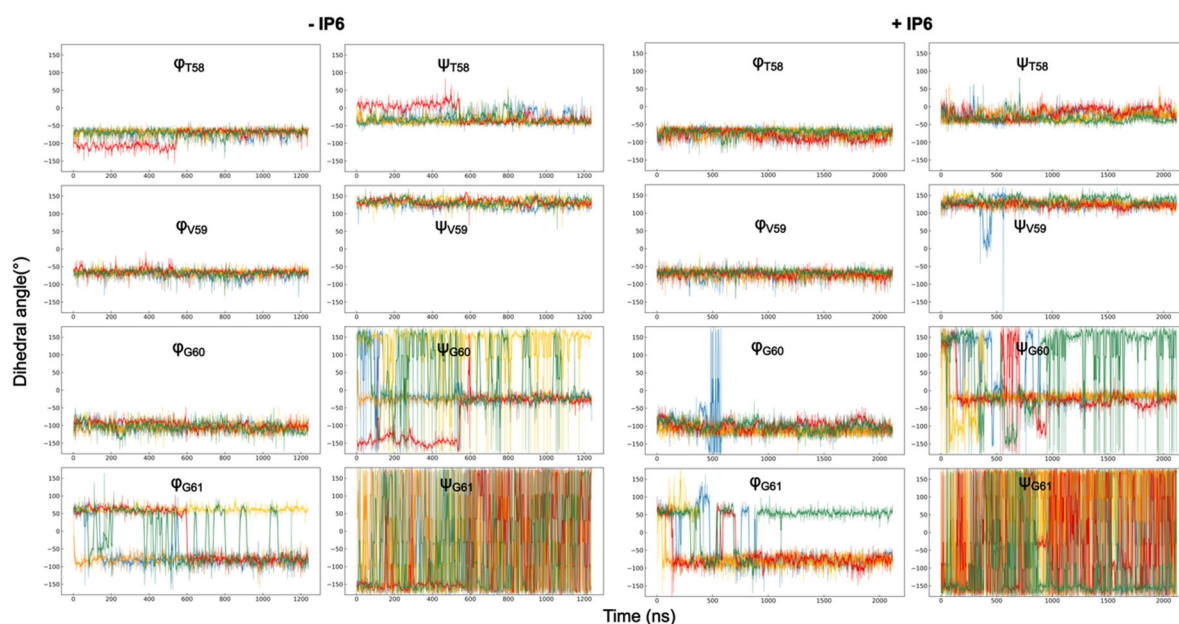


Fig. S5. Time series of the TVGG backbone dihedral angles in the absence of IP₆ (-IP₆) and presence (+IP₆).

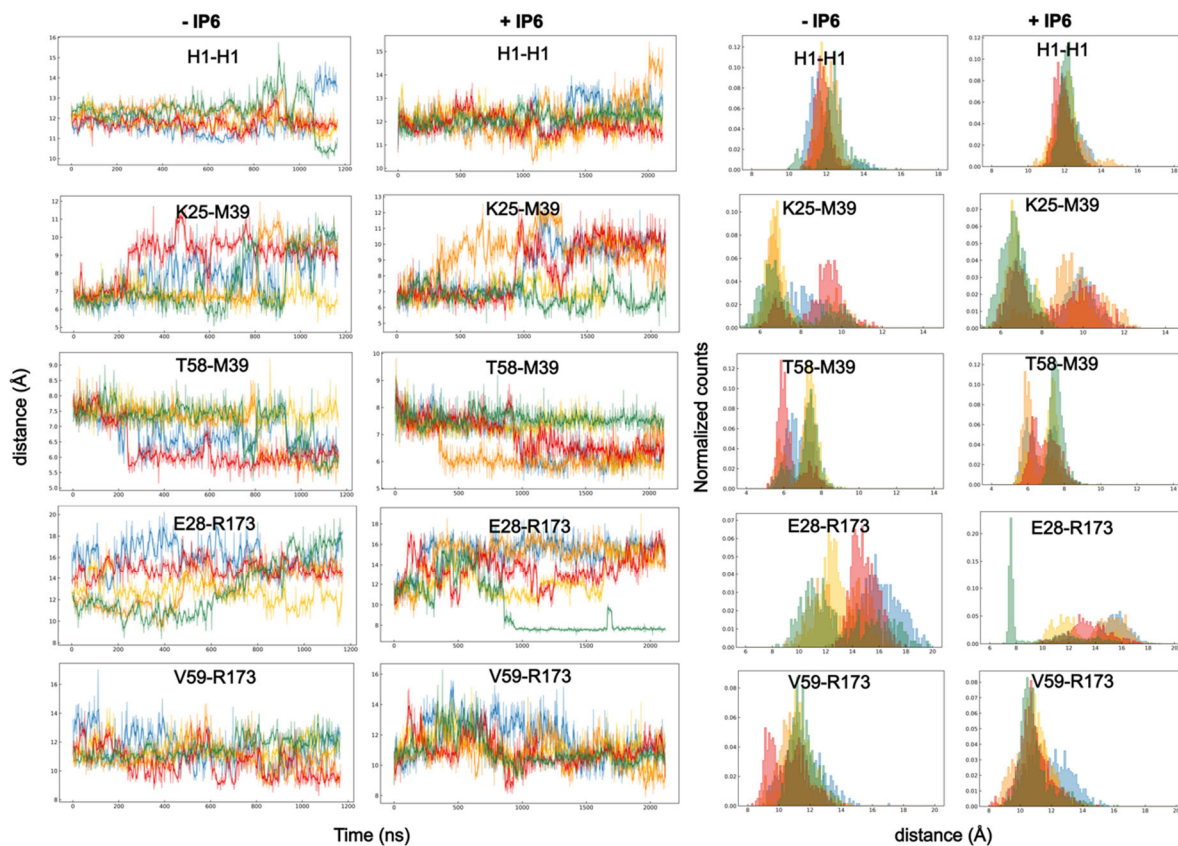


Fig. S6. Time series of the capsid structural network that links IP₆ to the TVGG motif in the absence (-IP₆) and presence (+IP₆) of IP₆. (-IP₆) The central pentamer pore was disordered, leading to the deviation of M39 residues from the 'pawl' conformation in multiple CA domains. (+IP₆) No major coil-to-helix transition was observed in this case since multiple CA domains in the IP₆-bound pentamer slipped into the 'ratchet' state.

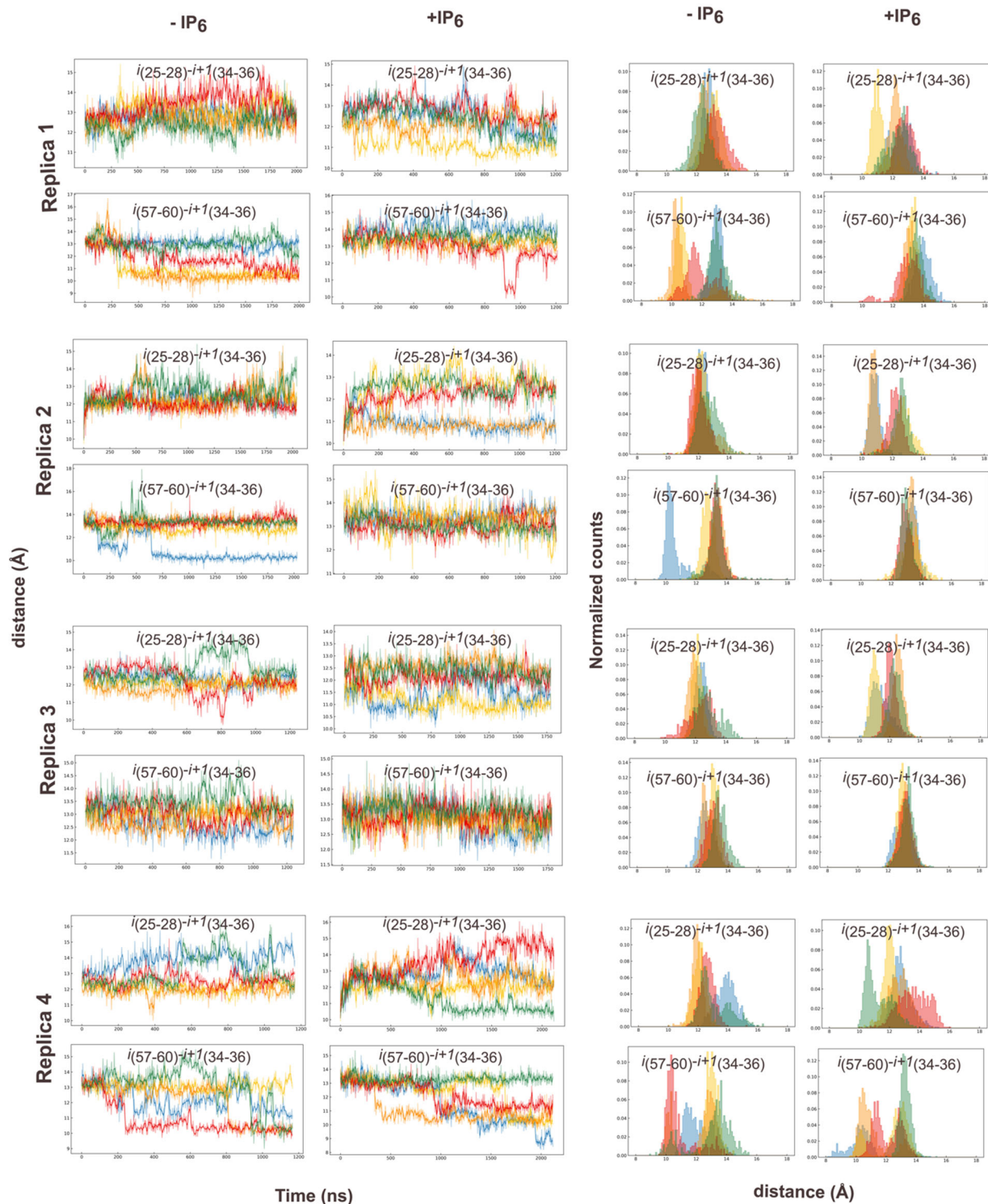
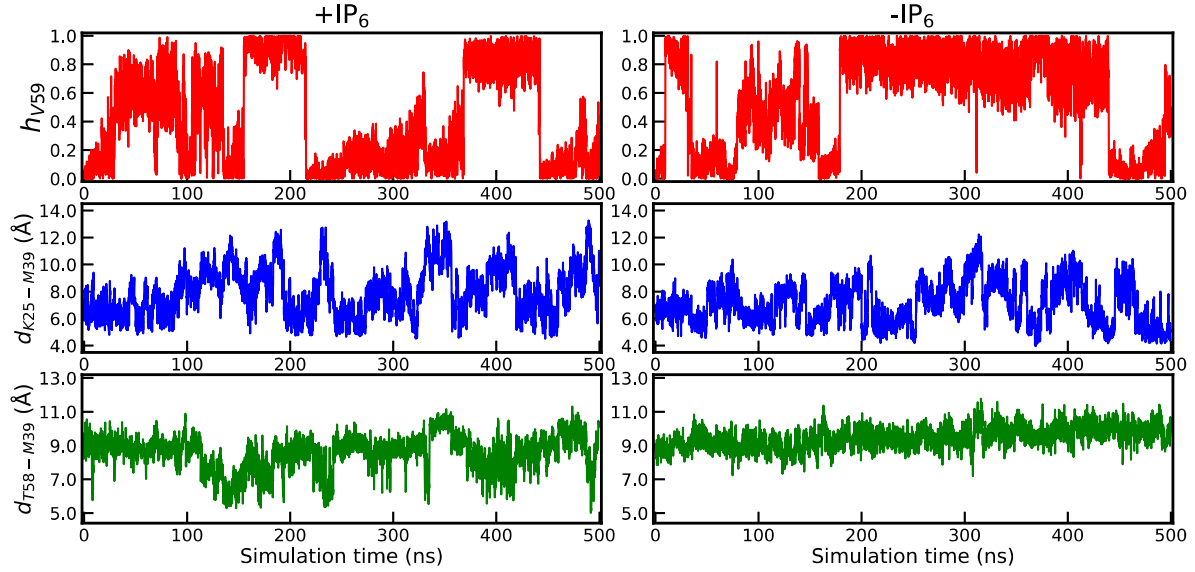


Fig. S7. Comparison of hydrophobic core of the Pentamer NTD in the absence (-IP6) and presence (+IP6) of IP6. (A) Color map of contacts between helix 1 and neighboring helix 2 (top) and time series of distance between residues 25-28 of helix 1 and 34-36 of adjacent helix 2 (bottom). **(B)** Contact map for (+IP6) simulations revealed interaction between the base of helix 1

and helix 2 (top), time course of residues 25-28 of helix 1 and 34-36 of adjacent helix 2 (bottom). **(C)** the base of CA helix 3 moves toward helix 2 of adjacent NTD adopting a hexamer-like state in the absence of IP₆ (top), time series analysis shows helix 3 of CA_i contacting helix 2 of CA_{i+1} (bottom). **(D)** Pentamer NTD-NTD interface is preserved in (+IP₆)-simulations.

Replica1



Replica2

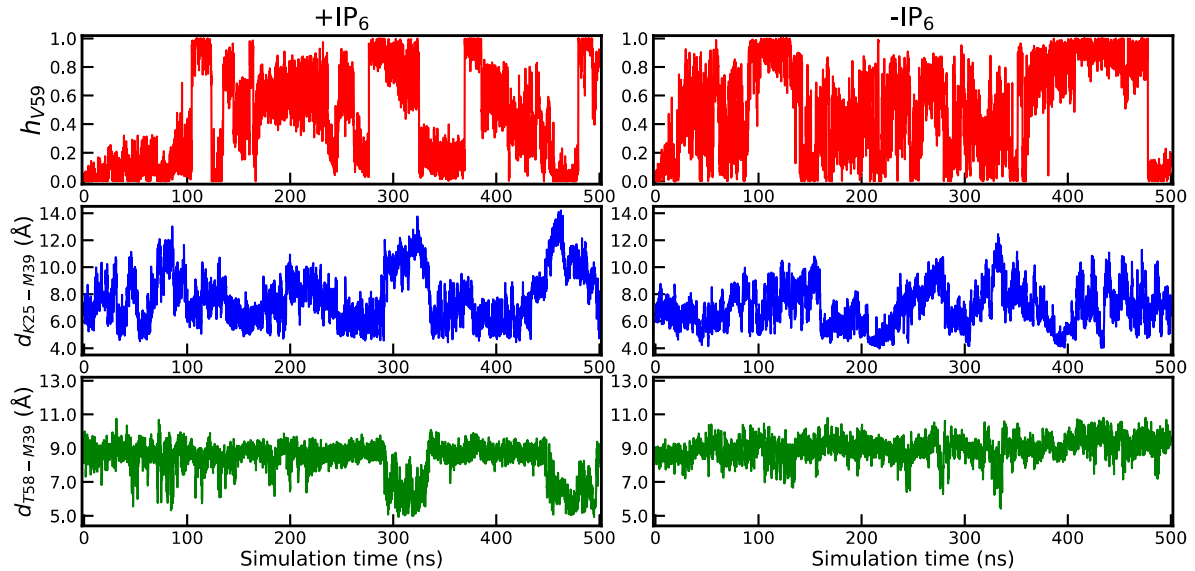


Fig. S8. Time series of the WT-MetaD simulation in the presence (+IP₆) and absence (-IP₆) of IP₆ bound to the pore. The time series of the helicity parameter (h_{V59}), the distance between K25 and M39 ($d_{K25-M39}$) of CA₁ and CA₂, and the distance between T58 and M39 ($d_{T58-M39}$) of CA₁ and CA₂, are shown in upper, middle, and lower panels, respectively.

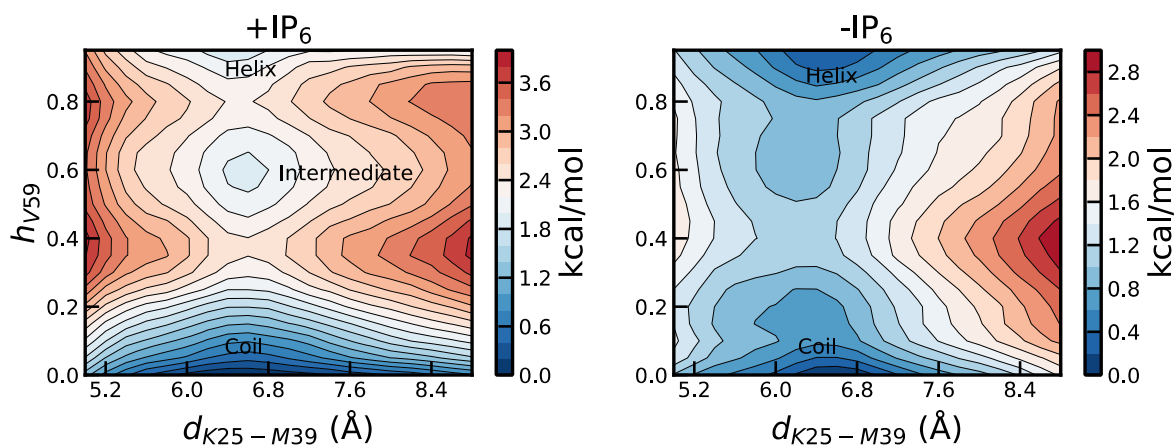


Fig. 9. Conformation landscape of the TVGG motif in the absence (-IP₆) and presence (+IP₆) of IP₆. 2-dimensional plot (Replica 2) of the PMF of the conformation landscape of the TVGG motif as a function of the helicity (h_{V59}) of V59, and distance between K25 of CA₁ and M39 of CA₂ denoted ($d_{K25-M39}$). The bar on the right has the color code for energy level contours in kcal/mole. The PMFs were calculated from the WT-MetaD simulations performed in the presence (+IP₆) and absence of (-IP₆). The PMFs of Replica 1 is shown in the main manuscript. The energy scale is 0.2 kcal/mol.

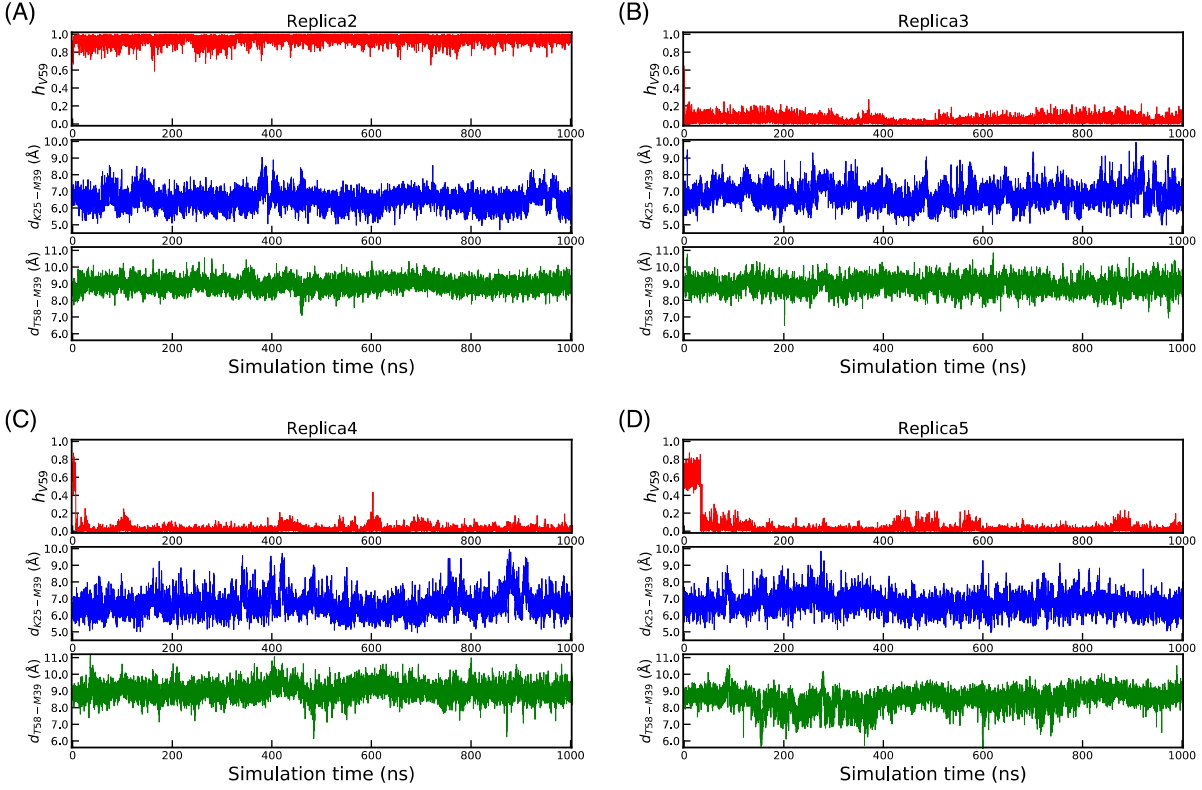


Fig. S10. Dynamics of coil-to-helix transition from the intermediate partially folded state. (A-D) Time evolution of the helicity parameter (h_{V59}), the distance between K25 and M39 ($d_{K25-M39}$) of CA_1 and CA_2 , and the distance between T58 and M39 ($d_{T58-M39}$) of CA_1 and CA_2 . The initial configuration corresponds to the intermediate partially folded state obtained from the WT-MetaD simulations in the presence of IP6. In the initial configuration of Replica2, the values of h_{V59} , $d_{K25-M39}$, and $d_{T58-M39}$ are 0.68, 6.5 Å, and 8.4 Å, respectively. In the initial configuration of Replica3, the values of h_{V59} , $d_{K25-M39}$, and $d_{T58-M39}$ are 0.64, 6.5 Å, and 8.8 Å, respectively. In the initial configuration of Replica4, the values of h_{V59} , $d_{K25-M39}$, and $d_{T58-M39}$ are 0.55, 6.1 Å, and 8.9 Å, respectively. In the initial configuration of Replica5, the values of h_{V59} , $d_{K25-M39}$, and $d_{T58-M39}$ are 0.58, 6.5 Å, and 8.7 Å, respectively.

Movie S1: Dynamics of the central pore of the capsid pentamer in the absence of IP₆ (-IP₆).

The pentameric central pore contains R18 and K25 rings, each made of five electropositive residues in proximity. The pore radius is smaller for the R18 ring compared to the K25 ring. In both rings, the sidechains fluctuate rapidly to decrease the repulsive force within the ring by orienting the positive charges in opposite directions. This increases the fluctuation within the central ring.

Movie S2: Dynamics of the central pore of the capsid pentamer in the presence of IP₆ (+IP₆).

In IP₆-bound pentameric, IP₆ coordinates the positive charges in the R18 and K25 rings to stabilize the central pore. Thus, the sidechain fluctuations in both rings are neutralized, bringing overall order to the pore. Electropositive sidechains in both rings point toward the center of the ring.